DALAT UNIVERSITY JOURNAL OF SCIENCE Volume 13, Issue 1, 2023 30-44

INFLUENCE OF STRUCTURAL PARAMETERS ON OPTICAL CHARACTERISTICS OF PHOTONIC CRYSTAL FIBERS WITH CIRCULAR LATTICE

Dang Van Trong[a], Le Tran Bao Tran[a], Chu Van Lanh[a], Nguyen Thi Hong Phuong[b], Trang Nguyen Minh Hang[c], Hoang Trong Duc[d], Nguyen Thi Thuy[d*]

[a]Department of Physics, Vinh University, Nghe An, Vietnam
[b]Nguyen Chi Thanh High School, Tay Ninh, Vietnam
[c]IGC Tay Ninh School, Tay Ninh, Vietnam
[d]The Faculty of Physics, University of Education, Hue University, Thua Thien Hue, Vietnam
[*]Corresponding author: Email: ntthuy@hueuni.edu.vn

Article history
Received: January 30th, 2022
Received in revised form: April 10th, 2022 | Accepted: April 25th, 2022
Available online: October 4th, 2022

Abstract

We demonstrate in this study that near-zero, ultra-flattened chromatic dispersion can be achieved over a wide range of wavelengths in photonic crystal fibers (PCFs) by means of slight variations in the geometrical parameters of the cladding. To do that, a new solid-core circular PCF design with various air hole diameters and lattice constants is presented, and the design features are numerically analyzed in detail. After 40 simulations, we determined three structures that possess optimal dispersion with the following lattice constants (Λ) and filling factors for the first ring (d_1/Λ): Λ = 0.8 µm, d_1/Λ = 0.45 for #F1, Λ = 0.9 µm, d_1/Λ = 0.45 for #F2, and Λ = 1.0 µm, d_1/Λ = 0.45 for #F3. High nonlinearity and low attenuation are outstanding features of our model. With these advantages, the proposed fibers are targeted for smooth flat broadband supercontinuum generation for near-infrared applications.

Keywords: Circular photonic crystal fibers; High nonlinearity; Low attenuation; Near-zero ultra-flattened dispersion.

DOI: https://doi.org/10.37569/DalatUniversity.13.1.1025(2023)

Article type: (peer-reviewed) Full-length research article

1. INTRODUCTION

Photonic crystal fiber (PCF) (Knight et al., 1996), also called microstructured fiber or holey fiber, is a special class of optical fiber capable of controlling the propagation of light. The fibers are fabricated based on the properties of photonic crystals with a periodic refractive index distribution over the fiber cross-section (Knight, 2003; Russell, 2003). Unlike conventional fibers, PCF contain micro-holes that run along the fiber axis and surround a central defect region that serves as a core. Based on their structure, PCFs can be classified as index-guiding or as photonic bandgap fibers, and all characteristics of PCFs are derived from the presence of air holes in the cladding.

Microstructured optical fiber has attracted widespread interest throughout the scientific community due to its compatibility with functional materials and flexible design with endless single-mode transmission (Birks et al., 1997), high birefringence (Su et al., 2014), tailorable chromatic dispersion (Saitoh et al., 2003, 2005), and nonlinear controllability (Hilligsøe et al., 2004). Since the first appearance of PCFs, research on their uses has changed almost all branches of optics, resulting in many potential applications, such as high-power laser delivery (Humbert et al., 2004), optical sensing fibers (Jin et al., 2010; Wang et al., 2010), dispersion compensating fibers (Birks et al., 1999; Haque et al., 2014), interferometry (Vergnole et al., 2005), polarization controllers, etc. PCFs are very interesting for nonlinear applications because of dispersion management techniques and high confinement of the optical field over long distances (Buczynski et al., 2011; Hansen, 2003; Rasmussen et al., 2006). These are the key factors affecting the performance of supercontinuum (SC) generation. SC generation is most efficient when the fibers have a flat, near-zero dispersion profile, maximum nonlinearity, minimal loss, and effective mode area. In order to gain these properties, many designs with various shapes, sizes, and spacing of the holes have been proposed and analyzed (Le et al., 2020; Medjouri et al., 2015; Nguyen et al., 2022; Pandey et al., 2021; Pniewski et al., 2016; Stepniewski et al., 2016; Vo et al., 2021). A proper choice of these parameters provides the desired optical features of PCFs.

In addition, further modification of the guiding properties of a PCF is possible by changing the air hole arrangement in the cladding microstructure. The lattice created in the coating is usually hexagonal, circular, square, triangular, or pentagonal. It is known that the SC spectrum expansion of circular PCFs is better than for others with the same set of geometrical parameters and material owing to the high symmetry that causes light to be strongly confined in the core. PCFs with a circular structure have been intensively studied to date (Ahmad et al., 2016, 2020; Amir et al., 2013; Luke et al., 2016; Maji & Chaudhuri, 2013; Saghaei & Ghanbari, 2017) and significant improvements, including high negative dispersion, increased nonlinearity, low confinement loss, flattened chromatic dispersion, ultra-wideband supercontinuum spectra, etc., have been made through the control of lattice parameters. However, in most of the investigated fibers, the air holes in the lattice rings have a single diameter. Although these traditional configurations are easy to fabricate, they cannot optimize the dispersion and loss characteristics simultaneously. Besides, the distance between the hole rings in the cladding also drastically influences the transmission features of the fibers.

With the difference between air hole diameters and lattice constants of the innermost ring and the outer rings, the silica-based, solid-core circular photonic crystal fiber proposed in our work can provide a viable solution to enhance the fiber's nonlinearity. With this configuration, it is possible to attain a broadband, ultra-flat, near-zero dispersion range and a high nonlinear coefficient along with extremely small attenuation. We organize the rest of this article as follows. In Section 2, we present the basic theory of light propagation in PCFs. The design process of the proposed PCFs, which uses commercial Lumerical MODE Solutions software, is described in Section 3. Section 4 discusses the numerical results used to find optimal structures for normal and anomalous dispersion regimes. Finally, we conclude the paper by summarizing our results in Section 5.

2. THEORETICAL ANALYSIS

The preliminary simulation of the optical characteristics of the guided modes is performed using the full-vectorial finite element method (Brechet et al., 2000), which divides the cross-section of the fiber into a patchwork of rectangular elements. Then, the effective indices $n_{eff} = \beta / k_0$ are obtained by solving an eigenvalue problem in the form of $E = E(x, y)e^{-i\beta z}$, where β is the propagation constant of a PCF, E is the electric field, and $k_0 = 2\pi / \lambda$ denotes the free space wavenumber. The electromagnetic wave propagation is described by Equation (1) (Saitoh & Koshiba, 2002):

$$\nabla \times \left(\frac{1}{\mu_r} \nabla \times E \right) - k_0 \varepsilon_r E = 0 \tag{1}$$

where μ_r is permeability and ε_r is permittivity. We assume anisotropic perfectly matched layers (absorbing boundaries) positioned outside the computational window to account for the leakage property of the modes. Dispersion $D(\lambda)$, also known as the temporal pulse broadening, is an important optical feature for nonlinear optical applications. As with standard fiber, the chromatic dispersion of a PCF includes waveguide and material dispersion. The waveguide dispersion can substantially affect the total fiber dispersion since the photonic structure is very complex. Additionally, one can mathematically relate the dispersion parameter to the group velocity dispersion (GVD) by solving the Maxwell equation (Agrawal, 2013):

$$D(\lambda) = -\frac{2\pi c}{\lambda^2} \beta_2 = -\frac{\lambda}{c} \frac{d^2 \,\mathrm{Re}[n_{eff}]}{d\lambda^2} \tag{2}$$

in which β_2 is the second-order dispersion coefficient that is related to the GVD parameter, Re[n_{eff}] represents the real part of the effective refractive index at wavelength λ for each mode, and c is the speed of light in a vacuum. Both the normal ($D < 0$) and anomalous ($D > 0$) dispersion states are considered here. The wavelength at which D is canceled is called the zero-dispersion wavelength (ZDW).

Another key issue during SC generation analysis is to design the nonlinear coefficient (γ) to be as high as possible. It occurs owing to the interaction of intense light with glass due to the contribution of the Kerr and Raman effects and is given by (Agrawal, 2013), where n_2 is the nonlinear refractive index of the fiber background material, λ_0 is the center wavelength, and $A_{eff}(\lambda)$ is the effective cross-sectional area representing the field distribution of the mode within the PCF core:

$$\gamma = \frac{2\pi}{\lambda}\frac{n_2}{A_{eff}} \tag{3}$$

$$A_{eff}(\lambda) = \frac{\left(\iint |E(x,y)|^2\, dxdy\right)^2}{\iint |E(x,y)|^4\, dxdy}. \tag{4}$$

3. DESIGN AND DEVELOPMENT OF THE PCF STRUCTURE

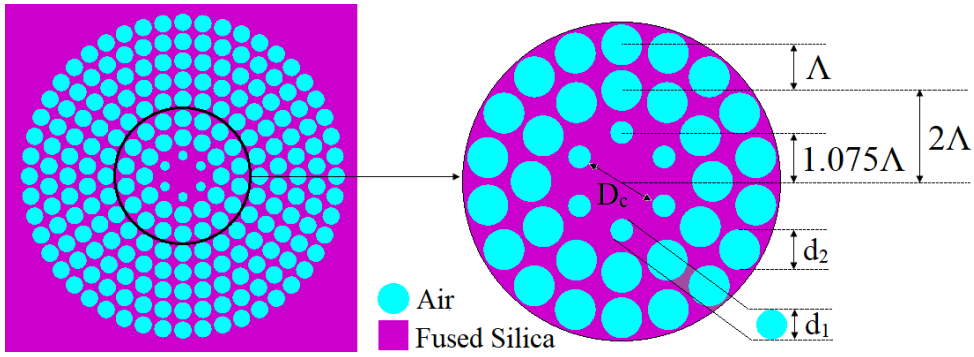

Figure 1. Geometry of the silica-based PCF structure with a circular lattice

The goal of this section is to design a suitable air-glass structure that allows optimization of the mode parameters of the fiber. In doing so, we examine a typical PCF developed and fabricated using conventional stack-and-draw technology. The PCF is formed by assembling fused silica capillaries into a preform "stack," and the sub-preform is then inserted into a sleeve tube and drawn into fiber (Suzuki et al., 2001). Because longitudinal homogeneity is needed for the air hole array in the PCF, precise control of the drawing parameters (pulling temperature and speed) during this stage is crucial to preserve the intended size of the air holes. A schematic of the final fiber is shown in Figure 1, where three rings of air holes are depicted for clarity. The real PCF consists of microstructured cladding with eight rings of air holes characterized by two parameters, the linear filling factor d/Λ and the lattice constant Λ, surrounding a solid core of diameter D_c. Various air-filling factors are used for the first ring of holes (d_1/Λ = 0.3–0.75), where d_1 is the diameter of the air holes in this ring. For the second ring onwards, the air holes have the same diameter $d_2 = 0.9\Lambda$. Our model originates from the results in Saitoh et al. (2003), where the authors discussed the dependence of the dispersion characteristics of the guiding mode on the lattice parameters (dispersion regime, flatness, and ZDW shift) in the first ring around the core. Mode attenuation, even in the higher modes, is dominated

by the remaining outer rings. Not only do we change d_1/Λ, but we also induce heterogeneity in the lattice constant of the photonic cladding. Specifically, the distance from the center of the first ring of holes to that of the solid core is increased to satisfy $\Lambda_1 = 1.075\Lambda$, which means that the first and second rings are only 0.925Λ apart because the value of 2Λ is kept constant. The dimension of the fiber core is now calculated by the formula $D_c = 2\times1.075\Lambda - d_1$. Simulations for modal properties in terms of effective refractive index, effective mode area, dispersion, and loss are investigated in the range of wavelengths determined by the available parameters of the material used.

In the current designs, we assume fused silica glass as the base material because of its high transparency and purity and its ease of use in fiber fabrication. The linear refractive index of fused silica as a function of wavelength is described via the Sellmeier relationship given in Equation (5), with the respective parameters listed in Table 1. In the following section, by controlling d_1/Λ and Λ, we successfully identify optimal structures with ultra-flat dispersion in a wide bandwidth (above 700 nm) and a very small value of attenuation. These are the advantages of our designs compared with those of previous studies (Amir et al., 2013; Maji & Chaudhuri, 2013; Saghaei & Ghanbari, 2017) that do not consider differences in the structural parameters of the coating.

$$n^2(\lambda) = B_0 + \frac{B_1\lambda^2}{\lambda^2 - C_1} + \frac{B_2\lambda^2}{\lambda^2 - C_2} + \frac{B_3\lambda^2}{\lambda^2 - C_3} \tag{5}$$

Table 1. Geometrical parameters of the proposed PCFs

Sellmeier coefficients	Values
B_0	1
B_1	0.6694226
B_2	0.4345839
B_3	0.8716947
C_1 [μm^2]	4.4801×10^{-3}
C_2 [μm^2]	1.3285×10^{-2}
C_3 [μm^2]	95.341482

4. NUMERICAL SIMULATIONS FOR OPTIMIZATION OF PCF CHARACTERISTICS FOR SUPERCONTINUUM GENERATION

Numerical analyses were carried out based on scanning electron microscopy images of the fibers for the lattice constants of 0.8 μm, 0.9 μm, 1.0 μm, and 1.5 μm. With the use of Lumerical MODE Solutions software, the relevant intensity distribution of the guided mode was obtained for a given wavelength. Figure 2 illustrates the patterns of the fundamental mode at 1.55 μm in two cases: the smallest core diameter D_{cmin} = 1.12 μm and the biggest one D_{cmax} = 2.775 μm. The penetration of the mode field into the cladding

is observed to decrease with an increase in core dimension. However, at this wavelength, the optical field is essentially tightly confined in the core region.

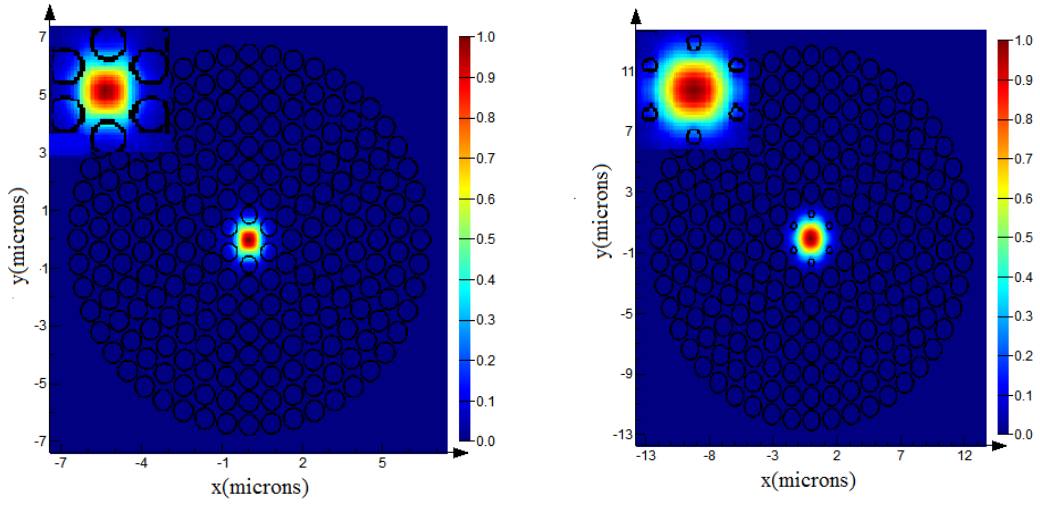

(a) (b)

Figure 2. Comparison of the simulated distributions of fundamental modes (in log scale) at 1.55 µm in the PCF with a) D_{cmin} and b) D_{cmax}

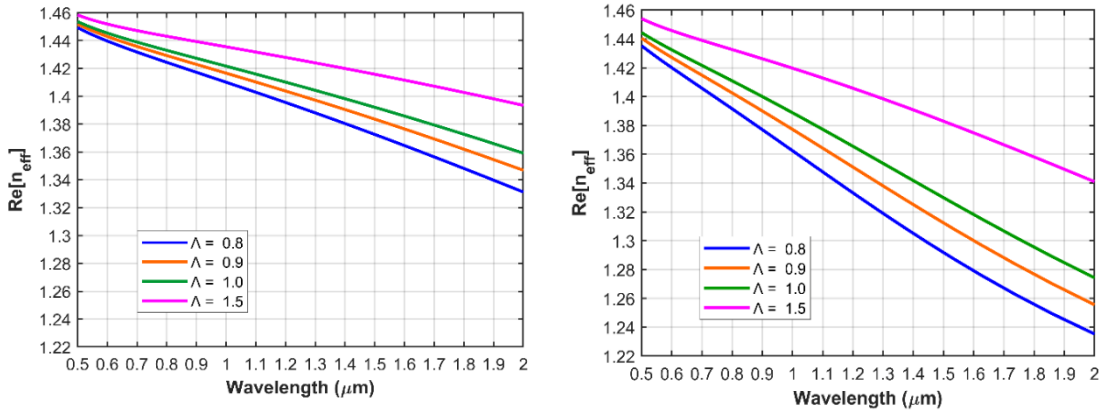

(a) (b)

Figure 3. Real part of the effective refractive index of circular PCFs with various lattice constants for filling factors of a) 0.3 and b) 0.75

The first step of the optimization process is presented in Figures 3 and 4, where we show the influence of the individual parameters on the total dispersion. Forty simulation runs were conducted at this stage. Figure 3 shows the real part of the effective refractive index n_{eff} of the base mode calculated for the PCFs with first ring filling ratios of 0.3 and 0.75. For all structures, changes in the wavelength, lattice constant, and filling factor lead to variations in the effective indices of refraction. The n_{eff} curves have a similar shape, decline monotonically with increasing wavelength, and rise for the PCFs with greater Λ. It should be noted that the structures corresponding to $d_1/\Lambda = 0.75$ possess a very low effective refractive index and an enormous slope compared to cases with a low

filling factor (d_1/Λ = 0.3) in the surveyed wavelength range. This is because the core of these fibers is very small, which results in a stronger interaction between light and the nonlinear medium (Figure 2). Figure 4 also clearly reveals that a combination of two effects, lattice constant and filling factor, augments the difference between the maximum and minimum dispersion values in the non-monotonic (or flat) region and changes the dispersion sign. Dispersion increases dramatically at short wavelengths: the slopes of the dispersion curves are large at wavelengths from 0.5 to 0.9 µm. If we take the intensification of Λ into account, we observe that the dispersion characteristics are flatter in the long-wavelength range, approach the zero axis, and eventually cross it once or twice. Alternatively, it can be asserted that the effect of waveguide dispersion on chromatic dispersion strengthens as the lattice constant decreases. This means that the total curves alter significantly, giving rise to diverse shapes of dispersion (Figure 4a).

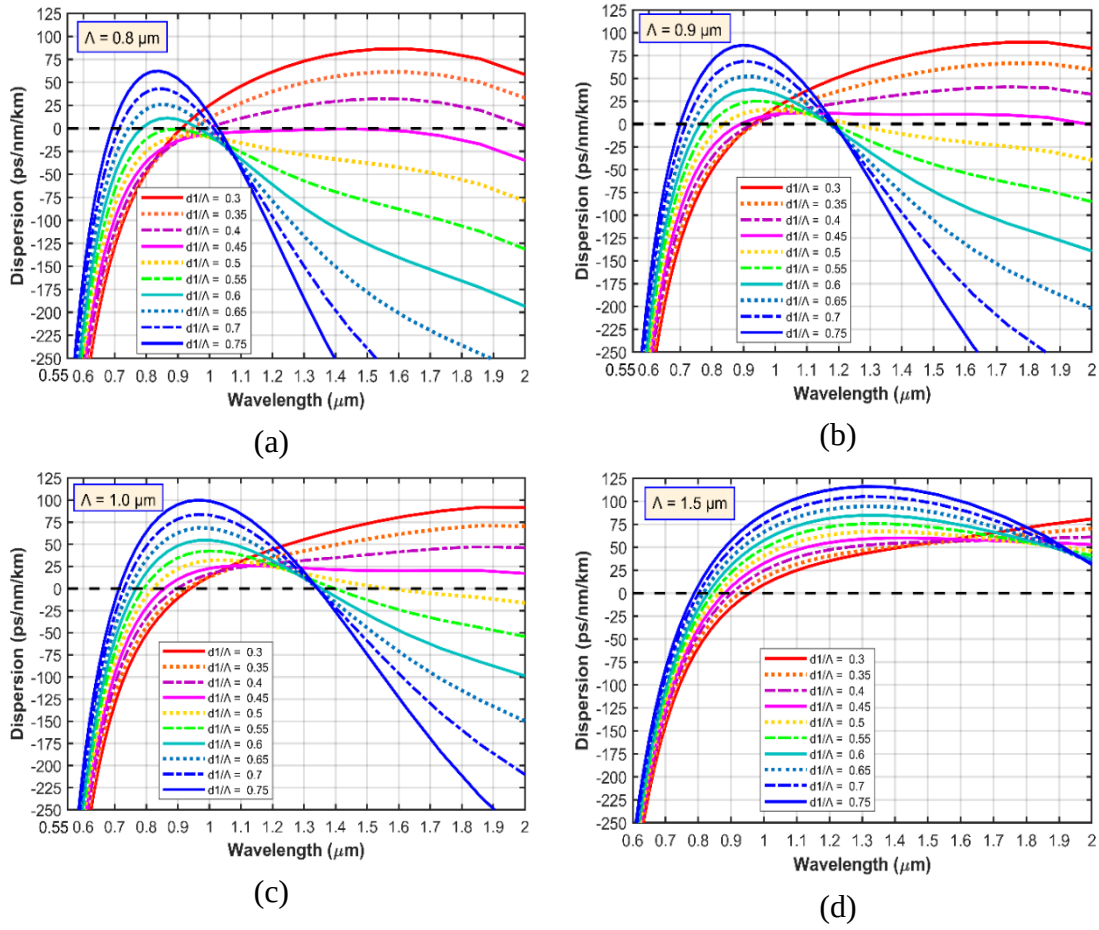

Figure 4. Plot of dispersion against wavelength for circular PCFs with Λ values of a) 0.8 µm, b) 0.9 µm, c) 1.0 µm, and d) 1.5 µm

Note: d_1/Λ varies from 0.3 to 0.75.

Almost all of the investigated structures have a ZDW except for the PCFs with a small core (Λ = 0.8 µm). In this case, three all-normal dispersion curves can be obtained that correspond to d_1/Λ = 0.45–0.55 of the filling factor, while no similarity is obtained

for other lattice constants. In particular, the structure with d_1/Λ = 0.45 possesses a very flat dispersion and is close to the zero-dispersion line over a wide range of wavelengths; this flatness is still maintained regardless of the regime change. As the core diameter is further enlarged, the PCFs operate in the dispersion region with one ZDW at low filling factor values and two ZDWs at higher values (Figures 4b and 4c). For Λ = 1.5 μm, the dispersion regime has only one ZDW in the wavelength range of interest because the effective refractive indices increase. The ZDW values of the different PCFs are summarized in Table 2. Obviously, by varying the structural parameters, we can achieve a very fine-tuning of ZDW. The strongest impact on the ZDW is seen in the small core fibers. For the large fibers, ZDW shifts toward longer wavelengths with a decrease in the filling factor of the first ring. This mechanism is extremely useful if we consider the application of PCFs for SC generation in the near-infrared region with low-cost, short-pulse microchip lasers.

Table 2. Zero-dispersion wavelengths (in μm) of PCFs with various Λ and d_1/Λ

d_1/Λ	Λ = 0.8 μm		Λ = 0.9 μm		Λ = 1.0 μm		Λ = 1.5 μm
	ZDW_1	ZDW_2	ZDW_1	ZDW_2	ZDW_1	ZDW_2	ZDW
0.3	0.991	-	0.883	-	0.94	-	0.956
0.35	0.946	-	0.937	-	0.927	-	0.927
0.4	0.992	-	1.04	-	0.896	-	0.902
0.45	-	-	0.891	1.985	0.857	-	0.881
0.5	-	-	0.837	1.24	0.821	1.566	0.862
0.55	-	-	0.796	1.179	0.791	1.397	0.845
0.6	0.785	0.996	0.764	1.171	0.767	1.356	0.83
0.65	0.743	0.993	0.739	1.173	0.747	1.343	0.815
0.7	0.714	1.013	0.718	1.181	0.729	1.341	0.801
0.75	0.691	1.028	0.7	1.188	0.713	1.342	0.788

In the next stage of the optimization, we choose three structures for generating nonlinear effects with low and flat dispersion and the possibility of switching between the dispersion states:

- #F_1: Λ = 0.8 μm, d_1/Λ = 0.45, D_c = 1.36 μm
- #F_2: Λ = 0.9 μm, d_1/Λ = 0.45, D_c = 1.53 μm
- #F_3: Λ = 1.0 μm, d_1/Λ = 0.45, D_c = 1.7 μm

The nonlinear properties of these PCFs have been studied in detail and are shown in Figures 5–8. Design #F_1 (blue curve in Figure 5) possesses a normal chromatic dispersion with an ultra-flat plateau roughly between 1000 nm and 1700 nm, but its core is smaller than that of the other fibers. The fact that most small-core designs have a high confinement loss over the long-wavelength range limits spectral broadening.

Nevertheless, SC generation with all-normal dispersion PCF has outstanding advantages that are widely aimed for since it makes the output pulses coherent, single, flat, and extensive when the pumped wavelength is close to the wavelength of the maximum dispersion. Although the fibers with d_1/Λ = 0.5 and 0.55 may also provide the same results, their curves show less flatness and are farther from the zero-dispersion line than that of the #F_1 fiber. Therefore, the structure with Λ = 0.8 µm, d_1/Λ = 0.45 is selected as one of the optimal fibers and is expected to pump at 1440 nm. In contrast, #F_2 and #F_3 fibers (red and pink curves) exhibit low anomalous dispersion for a wide range of wavelengths (up to 1000 nm) and have similar profiles. However, the difference in core size causes the dispersion curve of the #F_2 fiber to move in the negative direction and again intersect the zero-dispersion line at 1.985 µm (ZDW_2), while the ZDW of #F_3 is at about 0.857 µm. The central wavelengths of the laser pump source of these fibers are 0.88 µm and 0.85 µm, respectively, which are also the closest values to the ZDWs for all cases with Λ = 0.9 µm and 1.0 µm.

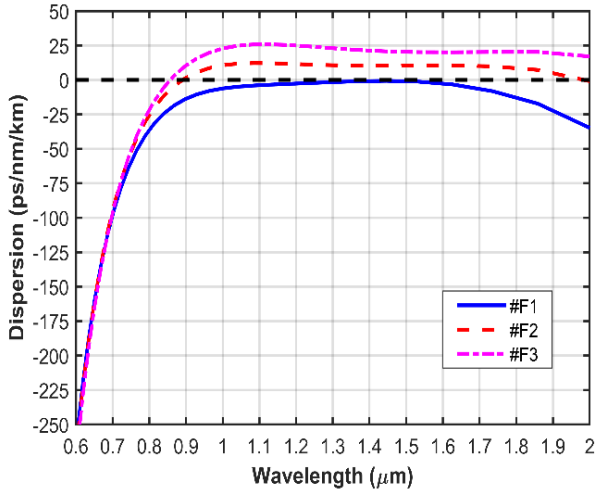

Figure 5. The chromatic dispersion of the selected structures

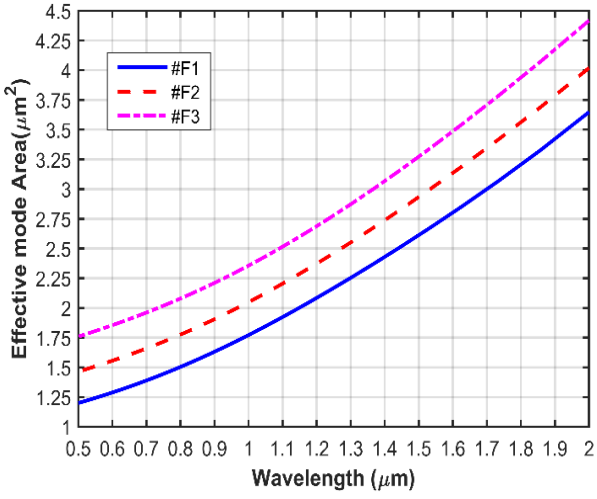

Figure 6. The effective mode area of the selected structures

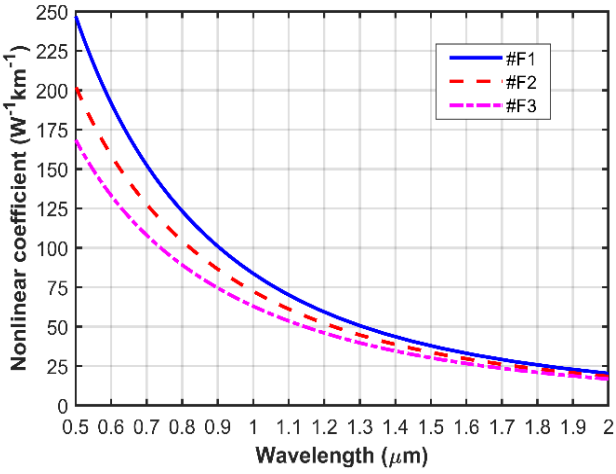

Figure 7. The nonlinear coefficient of the selected structures

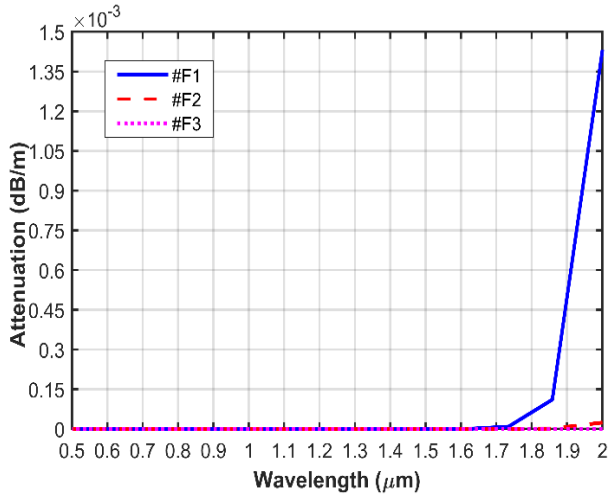

Figure 8. The attenuation of the selected structures

Besides the characteristics of the chromatic dispersion, the effective mode area and attenuation also determine the effective nonlinear medium for SC generation. Figure 6 shows that by increasing wavelength, the effective mode area A_{eff} increases for the three structures, and as a result, the nonlinear parameter will be reduced according to the relationship in Equation (3). As expected, A_{eff} of the #F1 fiber is smaller than those of the other PCFs because its core diameter is smallest. For this case, the cladding mode's effective refractive index is low, which strengthens the ability of local light, (i.e., the light field gradually moves away from the coating layer and increasingly concentrates in the core) leading effectively to decreases in A_{eff}. Furthermore, the biggest growth rate in A_{eff} is observed for the #F3 fiber (uplift by 2.66206 μm^2), followed by #F2 (2.55851 μm^2), and the smallest growth rate is observed for the first case, #F1 (2.45116 μm^2). The increase in the effective mode area is comparatively small, which is beneficial for nonlinear applications. The corresponding attenuation of these structures is displayed in Figure 8. Note that higher loss values arise at longer wavelengths, so that the low

attenuation windows are limited to the range from 0.5 to 1.6 μm for the three cases. Since the size of the core is relatively small compared to wavelengths greater than 1.7 μm, it leads to a sudden increase in the attenuation of the #F1 fiber. On the other hand, the #F3 fiber reveals the smallest loss and remains unchanged in a state almost coincident with the horizontal axis over the entire wavelength range, while the attenuation of $\#F_2$ rises slightly, but its increase is not significant compared with $\#F_1$. The attenuation of PCFs comprises not only the confinement loss but also a material loss. However, this value in our model is characterized mainly by the material loss of silica because the mode field is well restricted in the core.

Table 3. Characteristics calculated at the pump wavelength of structures #F1, #F2, #F3 and in previous publications

Optimized PCFs	Pump wavelength (μm)	D ($ps \cdot nm^{-1} \cdot km^{-1}$)	Attenuation (dB/m)	A_{eff} (μm^2)	γ ($W^{-1} \cdot km^{-1}$)
Amir et al. (2013)	1.55	About –20	2.357×10^{-10}	2.85	38.38
Chu et al. (2017)	1.55	–9.46	192	7.8	-
De and Singh (2019)	1.55	1.315	0.38538	9.537	12.7523
Nguyen et al. (2022)	1.55	1.502	202.5	10.497	-
Pandey et al. (2021)	1.55	–3.95	4.34×10^{-6}	4.86	25.03
$\#F_1$	1.44	–0.701	4.912×10^{-19}	2.502	41.186
$\#F_2$	0.88	–2.061	-1.228×10^{-20}	1.878	89.767
$\#F_3$	0.85	–2.258	-2.274×10^{-19}	2.143	81.433

The optical features of the proposed PCFs calculated at the pump wavelength are given in Table 3. From these results, it is seen that all three fibers have a rather low negative dispersion at the central wavelength of the input pulse; their values are –0.701 $ps \cdot nm^{-1} \cdot km^{-1}$, –2.061 $ps \cdot nm^{-1} \cdot km^{-1}$, and –2.258 $ps \cdot nm^{-1} \cdot km^{-1}$ for #F1, #F2, and #F3, respectively. The effective mode area of the #F1 structure is the largest, leading to its smallest nonlinear coefficient at 1.44 μm (equal to 41.186 $W^{-1} \cdot km^{-1}$), whereas at the pump wavelengths of 0.88 and 0.85 μm, the #F2 and #F3 values are twice as large as #F1. In addition, lower attenuation is witnessed for the #F2 and #F3 designs, corresponding to -1.228×10^{-20} dB/m and -2.274×10^{-19} dB/m, compared to 4.912×10^{-19} dB/m for the #F1 fiber. In general, with the variation in structural parameters, our designs achieve very flat dispersion curves and are closer to zero dispersion over a wide wavelength range than those of other projects (Amir et al., 2013; Chu et al. 2017; De & Singh, 2019; Luke et al., 2016; Nguyen et al., 2022; Pandey et al., 2021). This is an important property for generating coherent and noncoherent supercontinua with standard fiber femtosecond lasers, so we prioritized dispersion optimization first. We compare other quantities with those previously published to highlight the advantages of our designs. From Table 3 we can clearly see that the loss in our project is much smaller than in other studies. Amir et al. (2013), Chu et al. (2017), De and Singh (2019), Nguyen et al. (2022), and Pandey et al. (2021) have attenuation values of 2.357×10^{-10} dB/m, 192 dB/m, 0.38538 dB/m, 202.5

dB/m, and 4.34×10^{-6} dB/m, respectively. Moreover, our nonlinear coefficient value #F2 is three times higher than that of Pandey et al. (2021) and seven times higher than that of De and Singh (2019). The data are given in Table 3.

5. CONCLUSION

We present a novel model of a circular ring, microstructured PCF based on fused silica glass and numerically analyze its optical properties using the full-vectorial finite element method combined with a perfectly matched layer. A series of computer simulations is performed in which the diameter and lattice constant of the first core-neighborhood ring of air holes are varied. The simulations are performed to find structures with optimal dispersion shape and ZDW compatible with the pump source wavelength of the emission. Three such PCFs were obtained, providing near-zero, ultra-flattened, all-normal (#F1) and anomalous dispersion (#F2 and #F3). The results show that the structural parameters in the cladding do not only govern the chromatic dispersion but also improve the nonlinear properties of the PCFs, as desired, providing a small effective mode area, high nonlinearity, and low attenuation. PCFs with these parameters are very attractive and are good candidates for generating spectrally broad SC pulses.

ACKNOWLEDGMENTS

This research is funded by the Vietnam National Foundation for Science and Technology Development (NAFOSTED) under grant number 103.03-2020.03 and the Vietnam Ministry of Education and Training (B2021-DHH-08).

REFERENCES

Agrawal, G. (2013). *Nonlinear fiber optics (5th ed.)*. Elsevier. https://doi.org/10.1016/C2011-0-00045-5

Ahmad, R., Komanec, M., & Zvanovec, S. (2016). Circular lattice photonic crystal fiber for mid-IR supercontinuum generation. *IEEE Photonics Technology Letters*, *28*(23), 2736-2739. https://doi.org/10.1109/lpt.2016.2615657

Ahmad, R., Komanec, M., & Zvanovec, S. (2020). Ultra-wideband mid-infrared supercontinuum generation in liquid-filled circular photonic crystal fiber. *Journal of Nanophotonics*, *14*(2), 026016. https://doi.org/10.1117/1.JNP.14.026016

Amir, A., Revathi, S., Inbathini, S. R., & Chandran, A. (2013). Modeling of circular photonic crystal fiber structure for high non-linearity. *International Journal of Advanced Electrical and Electronics Engineering*, *2*(3), 88-92.

Birks, T. A., Knight, J. C., & Russell, P. St. J. (1997). Endlessly single-mode photonic crystal fiber. *Optics Letters*, *22*(13), 961-963. https://doi.org/10.1364/OL.22.000961

Birks, T. A., Mogilevtsev, D., Knight, J. C., & Russell, P. St. J. (1999). Dispersion compensation using single-material fibers. *IEEE Photonics Technology Letters*, *11*(6), 674-676. https://doi.org/10.1109/68.766781

Brechet, F., Marcou, J., Pagnoux, D., & Roy, P. (2000). Complete analysis of the characteristics of propagation into photonic crystal fibers, by the finite element method. *Optical Fiber Technology*, *6*(2), 181-191. https://doi.org/10.1006/ofte.1999.0320

Buczynski, R., Pysz, D., Stepien, R., Kasztelanic, R., Kujawa, I., Franczyk, M., Filipkowski, A., Waddie, A. J., & Taghizadeh, M. R. (2011). Dispersion management in nonlinear photonic crystal fibres with nanostructured core. *Journal of the European Optical Society – Rapid Publications*, *6*, 11038. https://doi.org/10.2971/jeos.2011.11038

Chu, V. L., Anuszkiewicz, A., Ramaniuk, A., Kasztelanic, R., Dinh, X. K., Cao, L. V., Trippenbach, M., & Buczyński, R. (2017). Supercontinuum generation in photonic crystal fibres with core filled with toluene. *Journal of Optics*, *19*(12), 125604. https://doi.org/10.1088/2040-8986/aa96bc

De, M. & Singh, V. K. (2019). Multi-purpose photonic crystal fiber having advanced optical properties and long sensing range. *Photonics and Nanostructures – Fundamentals and Applications*, *36*, 100722. https://doi.org/10.1016/j.photonics.2019.100722

Hansen, K. P. (2003). Dispersion flattened hybrid-core nonlinear photonic crystal fiber. *Optics Express*, *11*(13), 1503-1509. https://doi.org/10.1364/OE.11.001503

Haque, M. M., Rahman, M. S., Habib, M. S., & Razzak, S. M. A. (2014). Design and characterization of single mode circular photonic crystal fiber for broadband dispersion compensation. *Optik*, *125*(11), 2608-2611. https://doi.org/10.1016/j.ijleo.2013.11.063

Hilligsøe, K. M., Andersen, T. V, Paulsen, H. N., Nielsen, C. K., Mølmer, K., Keiding, S., Kristiansen, R., Hansen, K. P., & Larsen, J. J. (2004). Supercontinuum generation in a photonic crystal fiber with two zero dispersion wavelengths. *Optics Express*, *12*(6), 1045-1054. https://doi.org/10.1364/OPEX.12.001045

Humbert, G., Knight, J. C, Bouwmans, G., Russell, P. St. J., Williams, D. P., Roberts, P. J., & Mangan, B. J. (2004). Hollow core photonic crystal fibers for beam delivery. *Optics Express*, *12*(8), 1477-1484. https://doi.org/10.1364/OPEX.12.001477

Jin, W., Xuan, H. F., & Ho, H. L. (2010). Sensing with hollow-core photonic bandgap fibers. *Measurement Science and Technology*, *21*(9), 094014. https://doi.org/10.1088/0957-0233/21/9/094014

Knight, J. C. (2003). Photonic crystal fibres. *Nature*, *424*, 847-851. https://doi.org/10.1038/nature01940

Knight, J. C., Birks, T. A., Russell, P. St. J., & Atkin, D. M. (1996). All-silica single-mode optical fiber with photonic crystal cladding. *Optics Letters*, *21*(19), 1547-1549. https://doi.org/10.1364/OL.21.001547

Le, T. B. T., Nguyen, T. T., Vo, T. M. N., Le, C. T., Le, V. M., Cao, L. V., Dinh, X. K., Chu, V. L. (2020). Analysis of dispersion characteristics of solid-core PCFs with

different types of lattice in the claddings, infiltrated with ethanol. *Photonics Letters of Poland*, *12*(4), 106-108. https://doi.org/10.4302/plp.v12i4.1054

Luke, S., Sudheer, S. K., & Pillai, V. P. M. (2016). Tellurite based circular photonic crystal fiber with high nonlinearity and low confinement loss. *Optik*, *127*(23), 11138-11142. https://doi.org/10.1016/j.ijleo.2016.09.024

Maji, P. S., & Chaudhuri, P. R. (2013). Circular photonic crystal fibers: Numerical analysis of chromatic dispersion and losses. *International Scholarly Research Notices (ISRN Optics)*, *2013*, 986924. https://doi.org/10.1155/2013/986924

Medjouri, A., Simohamed, L. M., Ziane, O., Boudrioua, A., & Becer, Z. (2015). Design of a circular photonic crystal fiber with flattened chromatic dispersion using a defected core and selectively reduced air holes: Application to supercontinuum generation at 1.55 μm. *Photonics and Nanostructures – Fundamentals and Applications*, *16*, 43-50. https://doi.org/10.1016/j.photonics.2015.08.004

Nguyen, T. T., Hoang, T. D., Le, T. B. T., Dang, V. T., Chu, V. L. (2022). Optimization of optical properties of toluene-core photonic crystal fibers with circle lattice for supercontinuum generation. *Journal of Optics*. https://doi.org/10.1007/s12596-021-00802-y

Pandey, S. K., Singh, S., & Prajapati, Y. K. (2021). A novel PCF design with an ultra-flattened dispersion and low confinement loss by varying tiny air-hole concentration at core and cladding. *Optical Review*, *28*(2), 304-313. https://doi.org/10.1007/s10043-021-00662-8

Pniewski, J., Stefaniuk, T., Le, V. H., Cao, L. V., Chu, V. L., Kasztelanic, R., Stępniewski, G., Ramaniuk, A., Trippenbach, M., & Buczyński, R. (2016). Dispersion engineering in nonlinear soft glass photonic crystal fibers infiltrated with liquids. *Applied Optics*, *55*(19), 5033-5040. https://doi.org/10.1364/AO.55.005033

Rasmussen, P. D., Laegsgaard, J., & Bang, O. (2006). Chromatic dispersion of liquid-crystal infiltrated capillary tubes and photonic crystal fibers. *Journal of the Optical Society of America B*, *23*(10), 2241-2248. https://doi.org/10.1364/JOSAB.23.002241

Russell, P. (2003). Photonic crystal fibers. *Science*, *299*(5605), 358-362. https://doi.org/10.1126/science.1079280

Saghaei, H., & Ghanbari, A. (2017). White light generation using photonic crystal fiber with sub-micron circular lattice. *Journal of Electrical Engineering*, *68*(4), 282-289. https://doi.org/10.1515/jee-2017-0040

Saitoh, K., Florous, N., & Koshiba, M. (2005). Ultra-flattened chromatic dispersion controllability using a defected-core photonic crystal fiber with low confinement losses. *Optics Express*, *13*(21), 8365-8371. https://doi.org/10.1364/OPEX.13.008365

Saitoh, K., & Koshiba, M. (2002). Full-vectorial imaginary-distance beam propagation method based on a finite element scheme: Application to photonic crystal fibers. *IEEE Journal of Quantum Electronics*, *38*(7), 927-933. https://doi.org/10.1109/jqe.2002.1017609

Saitoh, K., Koshiba, M., Hasegawa, T., & Sasaoka, E. (2003). Chromatic dispersion control in photonic crystal fibers: Application to ultra-flattened dispersion. *Optics Express*, *11*(8), 843-852. https://doi.org/10.1364/OE.11.000843

Stepniewski, G., Kasztelanic, R., Pysz, D., Stepien, R., Klimczak, M., & Buczynski, R. (2016). Temperature sensitivity of chromatic dispersion in nonlinear silica and heavy metal oxide glass photonic crystal fibers. *Optical Materials Express*, *6*(8), 2689-2703. https://doi.org/10.1364/OME.6.002689

Su, W., Lou, S., Zou, H., & Han, B. (2014). Highly birefringent ZBLAN photonic quasi-crystal fiber with four circular air holes in the core. *Infrared Physics & Technology*, *66*, 97-102. https://doi.org/10.1016/j.infrared.2014.05.003

Suzuki, K., Kubota, H., Kawanishi, S., Tanaka, M., & Fujita, M. (2001). Optical properties of a low-loss polarization-maintaining photonic crystal fiber. *Optics Express*, *9*(13), 676-680. https://doi.org/10.1364/OE.9.000676

Vergnole, S., Delage, L., Reynaud, F., Labonté, L., Roy, P., Mélin, G., & Gasca, L. (2005). Test of photonic crystal fiber in broadband interferometry. *Applied Optics*, *44*(13), 2496-2500. https://doi.org/10.1364/AO.44.002496

Vo, T. M. N., Ho, D. Q., Le, T. T., Le, T. G., Le, C. T., Chu, V. L., Nguyen, T. T., Hoang, V. T., Nguyen, T. D., & Le, V. H. (2021). Numerical simulation of all-normal dispersion visible to near-infrared supercontinuum generation in photonic crystal fibers with core filled chloroform. *Hue University Journal of Science: Natural Science*, *130*(1B), 43-51. https://doi.org/10.26459/hueunijns.v130i1B.6243

Wang, Y., Tan, X., Jin, W., Ying, D., Hoo, Y. L., & Liu, S. (2010). Temperature-controlled transformation in fiber types of fluid-filled photonic crystal fibers and applications. *Optics Letters*, *35*(1), 88-90. https://doi.org/10.1364/OL.35.000088